

Revisiting the identity of -MgCl<sub>2</sub>: Part I. Structural disorder studied by synchrotron X-ray total scattering

*Original*

Revisiting the identity of -MgCl<sub>2</sub>: Part I. Structural disorder studied by synchrotron X-ray total scattering / Wada, T.; Takasao, G.; Piovano, A.; D'Amore, M.; Thakur, A.; Chammingkwan, P.; Bruzzese, P. C.; Terano, M.; Civalleri, B.; Bordiga, S.; Groppo, E.; Taniike, T.. - In: JOURNAL OF CATALYSIS. - ISSN 0021-9517. - 385:(2020), pp. 76-86. [10.1016/j.jcat.2020.03.002]

*Availability:*

This version is available at: 11583/2994192 since: 2024-11-08T16:17:16Z

*Publisher:*

Elsevier

*Published*

DOI:10.1016/j.jcat.2020.03.002

*Terms of use:*

This article is made available under terms and conditions as specified in the corresponding bibliographic description in the repository

*Publisher copyright*

(Article begins on next page)

# Revisiting the identity of $\delta$ -MgCl<sub>2</sub>: Part I.

## Structural disorder studied by synchrotron X-ray total scattering

*Toru Wada<sup>†,§</sup>, Gentoku Takasao<sup>†</sup>, Alessandro Piovano<sup>‡,§</sup>, Maddalena D'Amore<sup>‡</sup>,  
Ashutosh Thakur<sup>†</sup>, Patchanee Chammingkwan<sup>†,§</sup>, Paolo Cleto Bruzzese<sup>‡</sup>, Minoru Terano<sup>†,§</sup>,  
Bartolomeo Civalleri<sup>‡</sup>, Silvia Bordiga<sup>‡,§</sup>, Elena Groppo<sup>‡,§</sup> and Toshiaki Taniike<sup>\*,†,§</sup>*

<sup>†</sup>Graduate School of Advanced Science and Technology, Japan Advanced Institute of Science  
and Technology, 1-1 Asahidai, Nomi, Ishikawa, 923-1292, Japan

<sup>‡</sup>Department of Chemistry, INSTM and NIS Centre, University of Torino, Via Giuria 7,  
10125 Torino, Italy

<sup>§</sup>Dutch Polymer Institute, P.O. Box 902, 5600 AX Eindhoven, the Netherlands

KEYWORDS: Ziegler-Natta catalysts, structural disorder, nanocrystal, synchrotron, total scattering, XRD, pair distribution function

## ABSTRACT

The activation of  $\text{MgCl}_2$  is an essential step for preparing performant Ziegler-Natta catalysts (ZNCs), but the structural characterization of the so formed  $\delta\text{-MgCl}_2$  has been left behind due to its complicated disorder. In the current study, synchrotron X-ray total scattering is applied for the structure analysis of  $\delta\text{-MgCl}_2$ . Complementary use of powder X-ray diffraction (PXRD) and pair distribution function (PDF) enabled determining the type and extent of disorder for a series of mechanically and chemically activated  $\delta\text{-MgCl}_2$  samples. Moreover, their combination with molecular simulation successfully derived consistent nanoparticle models, where the conventional interpretation of disorderedly stacked nanoplates was justified in a cross-validated manner.

## 1. INTRODUCTION

In most of practical solid catalysts, one of the key features to control activity and selectivity [1–3], and in turn, to maximize performance of the catalyst is the lack of long-range order (i.e. periodicity). For instance, a nanosizing as one type of disorder leads to significant increment in the specific surface area and size-sensitive behaviors of electronic band structure, surface exposure, and phase morphology [1,4]. Since characterization of disordered materials is inherently less feasible [5], a careful validation on the basis of multi-aspect investigations is essential to uncover the hidden identity and catalytic relevance of structure disorder [2].

The  $\text{MgCl}_2$ -supported Ziegler-Natta catalysts (ZNCs) possess a dominant share in the industrial production of polyolefins. Their state-of-the-art form corresponds to multi-grained and porous spherical particles, those are composed by hierarchical aggregation of building blocks, called primary particles [6–12]. It is widely accepted that the primary particles are nanosized  $\text{MgCl}_2$  plates whose lateral surfaces are capped with  $\text{TiCl}_4$  and organic molecules (termed donors) [13]. Generally,  $\text{MgCl}_2$  is a crystalline compound, which is composed by stacking of ionic Cl-Mg-Cl tri-layers along the *c*-axis.  $\text{MgCl}_2$  has two polymorphs:  $\alpha$ - $\text{MgCl}_2$ , where Cl anions are stacked in the cubic close packing (ABCA), and less stable  $\beta$ - $\text{MgCl}_2$  with the hexagonal close packing (ABAB). On the other hand,  $\text{MgCl}_2$  in ZNCs exclusively displays a broad pattern of powder X-ray diffraction (PXRD), which is distinct from both of the polymorphs. The broadness of the  $\text{MgCl}_2$  PXRD pattern is deeply correlated with the performance of ZNCs. As a matter of fact, in the case of traditional mechanical routes (e.g. ball-milling  $\text{MgCl}_2$  with  $\text{TiCl}_4$  and donors), the broadness of the PXRD pattern and thus the catalyst activity develop along with the grinding time [14,15], while ZNCs prepared with modern chemical routes (e.g. through the precipitation of a  $\text{MgCl}_2$  solution, or through the solid-state conversion of  $\text{Mg}(\text{OR})_2$ ) exhibit even further broadened PXRD patterns and much better performance [16,17].

In the early 1980s, immediately after the discovery of  $\text{MgCl}_2$  as a support, the research groups of Zannetti and Giunchi individually explained the broad PXRD pattern of activated  $\text{MgCl}_2$  on the basis of stacking disorder. The idea was originally inspired by disorderedly stacked  $\text{TiCl}_3$  ( $\delta\text{-TiCl}_3$ ), and this became the origin of the term  $\delta\text{-MgCl}_2$ . They introduced structure models having mixed stacking sequences: ABCA for  $\alpha\text{-MgCl}_2$ , ABAB for  $\beta\text{-MgCl}_2$ , and ABCB or ABAC for rotationally disordered sequences. By tuning the probabilities of the three types of stacking sequences and crystallite dimensions, they successfully reproduced the broad PXRD patterns [18–20]. Since then, the structural analysis of  $\delta\text{-MgCl}_2$  has mainly relied on the interpretation of broad PXRD patterns based on the same concept [21,22], or more qualitatively based on the Scherrer equation [23–25]. Here, it must be noted that any kind of disorder such as random atomic displacements and lattice distortion distribution can cause broadening of PXRD patterns. The stacking faults and dimensional reduction are not the sole possible origin for the broad PXRD patterns of  $\delta\text{-MgCl}_2$ . For instance, Vittadello et al. proposed  $[\text{MgCl}_2]_n$  polymeric chains to reproduce the broad PXRD pattern of  $\delta\text{-MgCl}_2$ . This proposal was made in relation to the hypothesis that  $\text{MgCl}_2$  more or less memorizes the structure of the precursor [26]. Though such polymeric chains may not be thermodynamically stable, the idea must be equally probable to the conventional concept in term of explaining the broad PXRD pattern. To be most important, the lack of cross-validation based on analytical tools other than PXRD has caused this controversy on the structural identity of  $\delta\text{-MgCl}_2$ . Besides, the diffuse character of the PXRD pattern is potentially problematic for quantitative analysis, especially when laboratory XRD instruments are employed in Bragg-Brentano geometry [27–29].

Recently, structural analysis using an atomic pair distribution function (PDF) is becoming increasingly important in the field of nanomaterials [30]. The PDF expresses the existence probability of atomic pairs as a function of the distance between the atoms. It is a Fourier

transform of the structure function ( $S(Q)$ ) obtained via total scattering experiments using X-ray, neutron, or electron beams. The PDF allows to access real-space information through diffuse scattering. It is suitable for structural analysis of less ordered materials without intense Bragg diffraction, e.g. liquids, molten/amorphous metals or metal oxides, and nanomaterials. To be important, the PDF offers information at an intermediate distance ranging from 1 nm to several tens of nm, which is shorter than the periodicity required for XRD, but longer than the first or second coordination spheres that are accessible with NMR and extended X-ray absorption fine structure (EXAFS) spectroscopies. Thus, the PDF can be a powerful tool for structural analysis of  $\delta$ -MgCl<sub>2</sub>, but so far it has been applied only to an aqueous solution of MgCl<sub>2</sub> [31].

The purpose of the current study is to clarify the structural and morphological identity of  $\delta$ -MgCl<sub>2</sub> in a complementary manner [32]. So far, the structural features of  $\delta$ -MgCl<sub>2</sub> remain unknown not only due to its disorderliness, but also due to the historical lack of efforts in applying multilateral characterization on the “same” samples. In this regard, we employed a variety of characterization techniques specialized for the study of the disorder and atomic dynamics of  $\delta$ -MgCl<sub>2</sub> using the same set of samples. On the one hand, X-ray total scattering experiments using a synchrotron light source are first applied to a series of mechanically and chemically activated  $\delta$ -MgCl<sub>2</sub> samples. The crystallite dimensions and the extent of stacking disorder were determined by PXRD, and cross-validated with PDF analysis, and supported by simulation of well-defined MgCl<sub>2</sub> nanoparticle models. On the other hand, the same set of samples were successively investigated by Far-IR spectroscopy that, coupled with a state-of-the-art DFT study, provided relevant information on the morphology of the MgCl<sub>2</sub> nanoparticles and on the relative extension of the exposed surfaces [32]. The present contribution exclusively corresponds to the former part of this research for the analysis of the MgCl<sub>2</sub> disorder and crystallite size. By coupling this result with the latter part of the research

focused on the morphology and on the surface properties of the  $\delta$ -MgCl<sub>2</sub> [32], the state-of-the-art understanding on the structural and morphological identity of  $\delta$ -MgCl<sub>2</sub> is delivered in relation to primary particles of ZNCs.

## 2. EXPERIMENTAL AND THEORETICAL METHODS

### 2.1 Samples

A highly crystalline MgCl<sub>2</sub> sample was donated by Toho Titanium Co., Ltd. (MgCl<sub>2</sub> A, specific surface area: 9.3 m<sup>2</sup> g<sup>-1</sup>). In order to introduce the disorder, MgCl<sub>2</sub> A was subjected to planetary ball-milling, where 25 g was filled in a 0.5 L stainless-steel pot with 235 stainless-steel balls (10 mm diameter). The duration of the ball-milling was adjusted to make the specific surface area about five and eight times higher than that of MgCl<sub>2</sub> A, and thus obtained samples were termed as MgCl<sub>2</sub> B (specific surface area: 55 m<sup>2</sup> g<sup>-1</sup>) and MgCl<sub>2</sub> C (specific surface area: 73 m<sup>2</sup> g<sup>-1</sup>). A chemical reaction route from Mg(OEt)<sub>2</sub> was chosen as one of the most representative methods of chemical activation. The catalyst sample (hereafter termed ZNC) was prepared according to a patent [33] with small modifications [34–36], where *n*-dibutylphthalate (DBP) was used as an internal donor. The donor and Ti contents were determined as 14.1 wt% and 2.6 wt%, respectively. All the samples were handled and stored under an inert atmosphere in order to minimize the moisture adsorption.

### 2.2 PXRD and PDF measurements

#### 2.2.1 X-ray total scattering

X-ray total scattering experiments were performed at beamline BL5S2 in Aichi Synchrotron Radiation Center (AichiSR, Japan) with an X-ray energy of 20.7 keV ( $\lambda = 0.60$  Å). A capillary tube (0.3 mm internal diameter, Lindemann glass) was filled with a powder sample and flame-sealed under an inert atmosphere. The scattering intensities were obtained

by four 2D detectors in transmission geometry. Each of the detectors covers ca.  $15^\circ$  of  $2\theta$ , and the detectors moved in 5 positions to offer  $3\text{--}132^\circ$  as an entire  $2\theta$  range (corresponds to  $0.55$  to  $19 \text{ \AA}^{-1}$  in magnitude of the scattering vector,  $Q$ ). The 2D scattering data were converted to 1D data with software developed at AichiSR and the scattering intensity from an empty capillary was subtracted as the background. For the sake of direct comparison with literature, the diffraction angle was scaled to the wavelength of Cu K $\alpha$  radiation ( $\lambda = 1.5418 \text{ \AA}$ ).

### 2.2.2 MgCl<sub>2</sub> nanoparticle models

Nanoparticle models of MgCl<sub>2</sub> were created with the aid of DISCUS, where the conventional concept of stacking disorder and reduced crystallite dimensions was presumed unless specified [37]. A nanoparticle model was defined by four parameters:  $L_a$ ,  $L_b$ ,  $L_c$ , and  $P_c$ . The lateral dimensions ( $L_a$ ,  $L_b$ ) were determined by the number of unit cells repeated in the  $a, b$ -directions. The dimension in the basal direction ( $L_c$ ) corresponded to the number of Cl-Mg-Cl layers stacked along the  $c$ -direction. Stacking disorder was expressed by tuning the probability of  $\alpha$ -MgCl<sub>2</sub> sequence ( $P_c$ ) in a range of 25–100 %. The probabilities of  $\beta$ -MgCl<sub>2</sub> ( $P_h$ ) and rotational errors ( $P_{rot}$ ) were accordingly determined as follows:

$$P_h = (100 - P_c) \times 1/3,$$

$$P_{rot} = (100 - P_c) \times 2/3.$$

The lattice constants of the unit cell were set to  $0.3636 \text{ nm}$  ( $l_a$ ),  $0.3636 \text{ nm}$  ( $l_b$ ), and  $0.5889 \text{ nm}$  ( $l_c$ ). Here it must be noted that the periodicity along the  $c$ -direction is not clearly defined when stochastic stacking errors are included. Therefore,  $l_c$  was defined by the separation of neighboring Cl-Mg-Cl layers. The thickness of one Cl-Mg-Cl layer was set to  $0.2667 \text{ nm}$ . These values followed experimentally known lattice constants of  $\alpha$ -MgCl<sub>2</sub> [38], and it was found that the values were reasonably consistent with the obtained PXRD data irrespective of



the extent of the disorder. When the basal dimension of a nanoparticle model is small, such model does not contain a sufficient number of layers to determine the stacking probabilities. Therefore, an appropriate number of models were created at fixed dimensions, and simulated PXRD and PDFs were given as their averages. The presence of  $\text{TiCl}_4$  and DBP was omitted from the models due to the low Ti content (ca. 1.5 mol%), to the very low X-ray scattering power of the light atoms (H, C, and O), and to the random nature of the adsorption [39,40]. The software VESTA was used for visualization of the nanoparticle models [41].

### 2.2.3 PXRD simulation

For a given  $\text{MgCl}_2$  nanoparticle model, the PXRD pattern was simulated based on the Debye scattering equation with the aid of software DISCUS [37],

$$I_{calc}(Q) = \sum_i \sum_j f_i f_j \frac{\sin(2\pi Q r_{ij})}{2\pi Q r_{ij}} \quad (1),$$

where  $I(Q)$  is the scattering intensity as a function of  $Q$  ( $Q = 4\pi \sin\theta/\lambda$ ),  $f_i$  and  $f_j$  are the X-ray atomic scattering factors of atoms  $i$ th and  $j$ th, and  $r_{ij}$  is the distance between them. This equation represents the orientation-averaged scattering intensity from a nanoparticle model. As the equation rigorously incorporates peak broadening caused by finite crystallite sizes, it is suitable for the estimation of a PXRD pattern of nanoparticles [42]. The residual between a simulated pattern ( $I_{calc}(2\theta)$ ) and an experimental pattern ( $I_{exp}(2\theta)$ ) was calculated based on,

$$R_{w,PXRD} = \left[ \frac{\sum (I_{exp}(2\theta) - I_{calc}(2\theta))^2}{\sum I_{exp}(2\theta)^2} \right]^{\frac{1}{2}} \quad (2).$$

The model (i.e. the four parameters) was recursively updated in a way to minimize  $R_{w,PXRD}$ .

### 2.2.4 Acquisition of experimental PDF and PDF fitting

The obtained scattering data were converted into a reduced atomic pair distribution function ( $G_{exp}(r)$ ) using the software PDFgetX2 [43]. The 1D scattering data were corrected for X-ray polarization, Compton scattering, and X-ray atomic scattering factor to yield the total scattering structure function,  $S(Q)$ .  $G_{exp}(r)$  is derived by the Fourier transform of  $S(Q)$  [30],

$$\begin{aligned} G_{exp}(r) &= \left(\frac{\pi}{2}\right) \int_{Q_{min}}^{Q_{max}} [S(Q) - 1] \sin(Qr) dQ \\ &= 4\pi r [\rho(r) - \rho_0] \end{aligned} \quad (3),$$

where  $Q$  is the magnitude of the scattering vector,  $\rho(r)$  is the atomic pair density distribution, and  $\rho_0$  is the average atomic density. The  $Q_{max}$  and  $Q_{min}$  values in the Fourier transform were set to 15 and  $0.55 \text{ \AA}^{-1}$ , respectively.

The  $G_{exp}(r)$  was fit with simulated  $G_{calc}(r)$  with the aid of software PDFgui [44]. For a given nanoparticle model,  $G_{calc}(r)$  was calculated based on the following equations,

$$G_{calc}(r) = (G'_{calc} * S)(r) \quad (4),$$

$$G'_{calc}(r) = B(r) \left( \frac{1}{Nr} \sum_i \sum_j \left[ \frac{c_i c_j f_i f_j}{\langle f \rangle^2} T_{ij}(r) \right] - 4\pi r \rho_0 \right) \quad (5),$$

$$T_{ij}(r) = \frac{1}{\sqrt{2\pi}\sigma_{ij}} \exp \left[ -\frac{(r-r_{ij})^2}{2\sigma_{ij}^2} \right] \left[ 1 + \left( \frac{r-r_{ij}}{r_{ij}} \right) \right] \quad (6),$$

$$S(r) = \frac{\sin(Q_{max}r)}{r} \quad (7),$$

where  $N$  is the number of atoms in the nanoparticle model and  $c_i$  is the composition of  $i$ th element. The broadening factor  $\sigma_{ij}$  includes parameters for anisotropic displacement and correlation motion of atoms, and these parameters were optimized to minimize the residual function (for each nanoparticle model),

$$R_{w,PDF} = \left[ \frac{\sum (G_{exp}(r_i) - G_{calc}(r_i))^2}{\sum G_{exp}(r_i)^2} \right]^{\frac{1}{2}} \quad (8).$$

$B(r)$  incorporates a damping factor due to the finite instrument resolution. The  $Q_{\text{damp}}$  value was determined using a standard sample and fixed as constant in the fitting. The termination error due to the finite  $Q_{\text{max}}$  value was explained by  $S(r)$ .

The PDF simulation for nanosized materials using PDFgui is not straightforward as PDFgui requires a periodic boundary condition. In order to express the finite size effect, the following two strategies were employed in this study. When the model size was small (typically below 10 nm such as ZNC), the nanoparticle model was placed in a large cell. The separation between the neighbouring models was set to ca. 30 nm. The artificial effect of the vacuum region was subtracted by Dshaper [45]. When the model size was large (such as MgCl<sub>2</sub> B and C), the simulation based on the above strategy was prohibitively expensive. Instead, a shape function of Equation (9) was employed,

$$\gamma_{\text{Sphere}}(r, D) = \begin{cases} 1 - \frac{3}{2}\left(\frac{r}{D}\right) + \frac{1}{2}\left(\frac{r}{D}\right)^3 & (r \leq D) \\ 0 & (r \geq D) \end{cases} \quad (9),$$

where  $D$  is a fittable parameter to express the diameter of the model. This is a built-in function of PDFgui and widely applied for isotropic nanomaterials [46–48].

### 3. RESULTS AND DISCUSSION

#### 3.1 Simulation of PXRD patterns for a series of MgCl<sub>2</sub> models

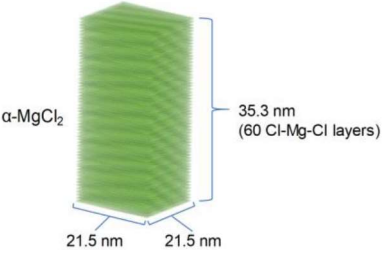
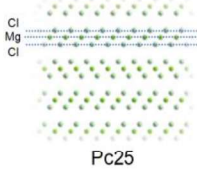
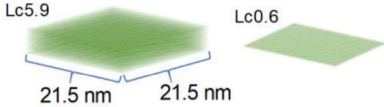
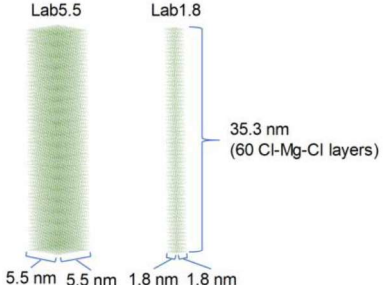
As the first step, we simulated PXRD patterns for a series of MgCl<sub>2</sub> nanoparticle models bearing different types of disorder. The disorder is classified into 1) stacking error along the  $c$ -axis, 2) thinning along the  $c$ -axis (decrease in the number of Cl-Mg-Cl layers), and 3) reduction of crystallite dimensions in the  $a, b$ -axes. A nanoparticle model with  $P_c = 100\%$ ,  $L_c = 35.3$  nm (60 layers) and  $L_{a,b} = 21.5$  nm was regarded as the least disordered nanoparticle model (hereafter termed as  $\alpha$ -MgCl<sub>2</sub>). Starting from this model, different types of disorder were separately introduced as shown in Table 1. In the 1st series, the stacking error was

increased by decreasing the  $P_c$  value from 100% (perfectly cubic) to 25% (random), while the other parameters were fixed at  $L_c = 35.3$  nm and  $L_{a,b} = 21.5$  nm. Similarly, the other two series were created by reducing the  $L_c$  value from 35.3 nm (60 layers) to 0.6 nm (monolayer) or by equally reducing the  $L_a$  and  $L_b$  values from 21.5 nm to 1.8 nm. Such simulation is believed to be useful for qualitative interpretation of featureless PXRD patterns of  $\delta$ -MgCl<sub>2</sub>, which has not been discussed earlier.

The simulated PXRD patterns are shown in Figure 1. It can be seen that each type of disorder has a unique impact on the PXRD pattern. The findings are listed as follows and summarized in Table 2.

- The stacking error does not affect the (003), (006), and (110) diffraction peaks because the dimensions of the crystallite in the basal and lateral directions are not altered. On the contrary, the diffraction peaks that relate to the structure repetition in the body-diagonal directions ((101), (012), (104), (107), and (018)) are significantly weakened and broadened along with the stacking error. Notably, the behavior of the (104) diffraction peak is unique as it is not only weakened and broadened but also shifts toward a smaller diffraction angle.
- The thinning in the  $c$ -axis diminishes the (003) and (006) diffraction peaks associated with the vertical direction as well as the peaks related to the body-diagonal direction. The (110) diffraction peak is slightly affected to make a tail toward a higher diffraction angle, which is typical for two-dimensional materials [49].
- The size reduction in the  $a,b$ -axes diminishes the (110) diffraction peak as well as the peaks related to the body-diagonal direction. The (003) and (006) peaks are almost unchanged.

**Table 1.** MgCl<sub>2</sub> nanoparticle models employed for the simulation of the PXRD and PDF patterns.<sup>a</sup>

Type of disorder	Name	$P_c$ [%]	$L_c$ [nm]	$L_a, L_b$ [nm]	Models
0	$\alpha$ -MgCl <sub>2</sub>	100	35.3	21.5 × 21.5	
1	Pc70	70	35.3	21.5 × 21.5	
	Pc55	55	35.3	21.5 × 21.5	
	Pc25	25	35.3	21.5 × 21.5	
2	Lc5.9	100	5.9	21.5 × 21.5	
	Lc2.9	100	2.9	21.5 × 21.5	
	Lc0.6	n.a.	0.6	21.5 × 21.5	
3	Lab5.5	100	35.3	5.5 × 5.5	
	Lab3.6	100	35.3	3.6 × 3.6	
	Lab1.8	100	35.3	1.8 × 1.8	

<sup>a</sup>The nanoparticle models are classified based on the disorder type as follows: **0** = standard structure; **1** = stacking error; **2** = thinning along the *c*-axis; **3** = size reduction along the *a, b*-axes.  $P_c$  = probability of  $\alpha$ -MgCl<sub>2</sub> sequence;  $L_c$  = dimension in the *c*-axis;  $L_a, L_b$  = dimension in the *a, b*-axes.

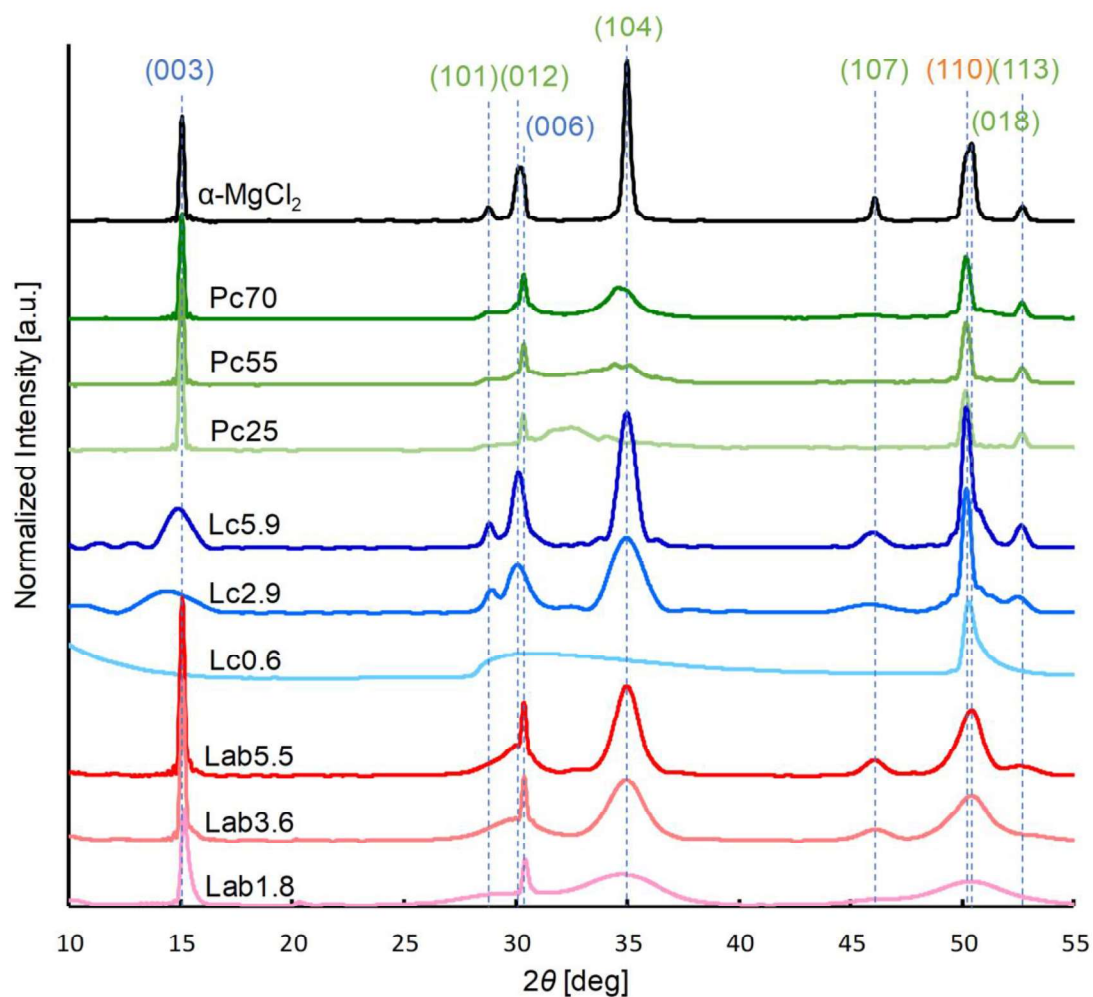


**Figure 1.** Simulated PXRD patterns for  $\text{MgCl}_2$  nanoparticle models with different types and extents of disorder (labels as in Table 1). The diffraction intensity is normalized by the number of atoms in individual models. The patterns are vertically translated for clarity.

**Table 2.** Impact of different types of disorder on the diffraction peaks, as determined by the simulated PXRD patterns shown in Figure 1.

$2\theta$ [deg]	Plane	Type of disorder <sup>a,b</sup>		
		1	2	3
15.1	(003)		++	
30.1	(012)	++	+	+
30.2	(006)		++	
35.0	(104)	++	+	+
50.2	(110)			++
50.4	(018)	++	++	+

<sup>a</sup> The type of disorder is numbered based on Table 1.

<sup>b</sup> ++: high impact, +: moderate impact, blank: no or marginal impact.

### 3.2 Analysis of the experimental PXRD patterns

As a second step, the PXRD patterns were extracted from the total scattering data (Figure 2). Due to the highly collimated nature and brightness of the light source, the extracted PXRD patterns displayed a high angular resolution as well as a remarkably high S/N ratio. Figure S1 shows comparison of PXRD patterns acquired at a synchrotron facility and a typical laboratory machine with Cu-K $\alpha$  radiation. In Figure 2, MgCl<sub>2</sub> A exhibited the diffraction peaks characteristic for  $\alpha$ -MgCl<sub>2</sub> ((003), (101), (012), (006), (104), (107), (110), (018), and (113)). In particular, the absence of the smaller-angle shift of (104) assured the scarcity of the stacking error, i.e. MgCl<sub>2</sub> A was safely regarded as  $\alpha$ -MgCl<sub>2</sub>. MgCl<sub>2</sub> B showed smaller intensities for (003) and (110) diffraction peaks together with a smaller-angle shift of (104), suggesting the occurrence of crystallite miniaturization and stacking error. This tendency was further enhanced for the even more ground MgCl<sub>2</sub> C. In the case of ZNC, the diffraction pattern became largely featureless. The (003) peak almost disappeared and slightly

shifted to a smaller angle. From the simulation results shown in Figure 1, the shift of the (003) peak was observed when the number of Cl-Mg-Cl layers was fewer than 10, and it completely disappeared for a Cl-Mg-Cl monolayer. Thus, the PXRD pattern shown in Figure 2 indicates that the crystallites in ZNC were composed of 2–10 layers. The (012) and (104) diffraction peaks completely merged to form a single broad peak, suggesting a large extent of stacking disorder. The sharpness of the (110) diffraction peak was comparable to that of Lab5.5 of the simulation results in Figure 2. Likewise, the crystallites of ZNC likely equipped all the types of disorder at higher extents than those characterizing the mechanically activated samples.

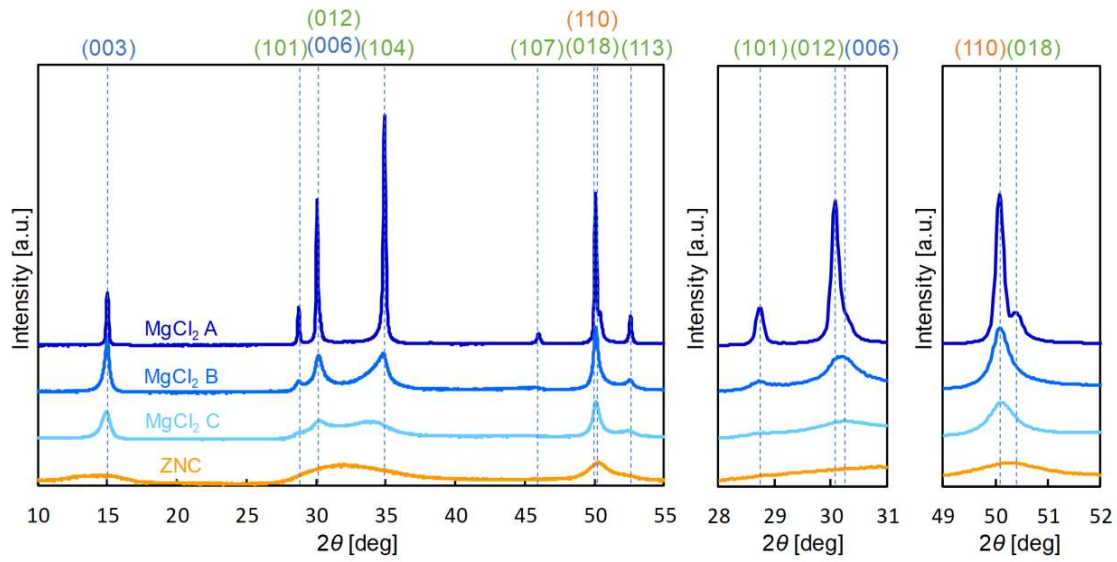


**Figure 2.** Experimental PXRD patterns of mechanically and chemically activated  $\delta$ -MgCl<sub>2</sub>.

Successively, a nanoparticle model was optimized in order to reproduce the experimental PXRD patterns. This was achieved by adjusting the four structural parameters ( $P_c$  and  $L_{A,B,C}$ ) to lower the fitting residual ( $R_{w,PXRD}$ ), except for MgCl<sub>2</sub> A. Indeed, the dimension of MgCl<sub>2</sub> A



was too large to calculate its PXRD pattern based on the Debye equation. Instead, the crystallite dimension was estimated from the full-width at half-maximum (FWHM) of the (003) and (110) diffraction peaks using the Scherrer equation [50] ( $D_{hkl} = 0.94\lambda\beta^{-1}\cos\theta^{-1}$ ,  $\lambda$ : X-ray wavelength,  $\beta$ : FWHM of the diffraction peak,  $\theta$ : diffraction angle of the peak). Comparison of the simulated and experimental PXRD patterns is shown in Figure 3. The four structural parameters of the best-fit nanoparticle models are summarized in Table 3, together with the fitting residual. The experimental PXRD patterns for MgCl<sub>2</sub> B and C could be well reproduced with the  $R_{w,PXRD}$  value of 0.196 and 0.152, respectively.  $P_c$  decreased from 100 % of MgCl<sub>2</sub> A to 64 and 43 % along the grinding, and the crystallite dimension eventually decreased to about 13 nm.

For ZNC, the (003) diffraction peak was hardly reproducible with any of the models which can be created by the four structural parameters. The addition of a new structural parameter such as the distribution in the thickness and the variation in the interlayer distance, moderately improved the fitting of the (003) peak, while it inevitably deteriorated the fitting in the other region. The origin of the deviation is yet unclear, but it is most likely attributed to overlapping contribution of so called small-angle scattering for the smallest crystallites of ZNC. Accordingly, we decided to exclude the smaller angle region below 20° of  $2\theta$  from the fitting, and this indeed led to an improved  $R_{w,PXRD}$  value of 0.068 as shown in Table 3. Even with the removal of the contribution of the (003) peak,  $L_c$  could be determined because it affects body-diagonal diffraction peaks as shown in Table 2. Thus determined nanoparticle model of ZNC was even smaller than that of MgCl<sub>2</sub> C. The crystallite consists of a few Cl-Mg-Cl layers with its lateral dimension below 10 nm and no stacking order ( $P_c = 25$  %).

All the fitting results reported in Table 3 were in good agreement with the qualitative observations. Notably, the experimental PXRD patterns of disordered  $\delta$ -MgCl<sub>2</sub> were well reproduced based on the conventional assumption of disorderedly stacked nanoplates,

irrespective of the method of activation. In the present work, the reliability of the fitting clearly improves when compared to previous literature [22], due to the utilization of a synchrotron light source.

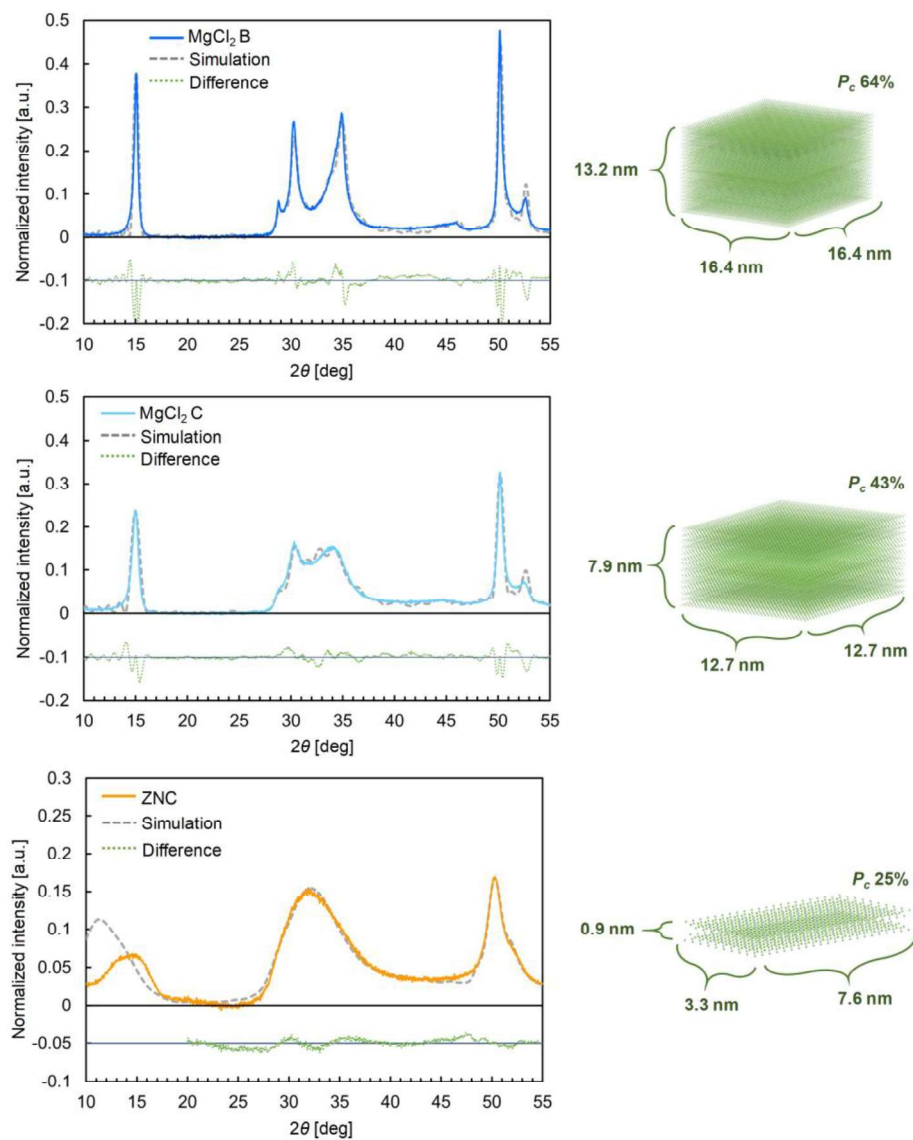


**Figure 3.** PXRD fitting results for MgCl<sub>2</sub> B, MgCl<sub>2</sub> C, and ZNC. The difference between the experimental and simulated patterns is shown as a green dotted line. The nanoparticle models based on the determined structural parameters are shown on the right side of each graph.

**Table 3.** Structural parameters and fitting residual for the best-fit of the experimental PXRD patterns

	MgCl <sub>2</sub> A <sup>a</sup>	MgCl <sub>2</sub> B	MgCl <sub>2</sub> C	ZNC (20–55°) <sup>b</sup>	ZNC (10–55°) <sup>b</sup>
$R_{w, PXRD}$	n.a.	0.196	0.152	0.068	0.132
$P_c$ [%]	100	64	43	25	25
$L_a$ [nm]	55	16.4	12.7	7.6	7.3
$L_b$ [nm]	55	16.4	12.7	3.3	3.6
$L_c$ [nm]	44	13.2	7.9	0.9	1.4

<sup>a</sup> PXRD simulation was not performed due to the large crystallite dimension.  $L_a$ ,  $L_b$ , and  $L_c$  were determined with the Scherrer equation.

<sup>b</sup> Fitting was performed over different  $2\theta$  ranges.

### 3.3 Simulation of PDF patterns for a series of MgCl<sub>2</sub> models

As in the case of PXRD, the impact of each structural parameter on the PDF patterns was first investigated using the same series of nanoparticle models reported in Table 1. The simulated PDFs up to 1.6 nm are summarized in Figure 4. The introduction of stacking error (Pc70-Pc25 series) weakens the features related to the cubic packing (e.g. 1.1 and 1.3 nm), while new features corresponding to the other types of packing appear at e.g. 1.05 and 1.45 nm. The damping along with the atomic distance  $r$  is induced by the thinning in the  $c$ -axis ( $L_c$  series) and the in-plane miniaturization ( $L_b$  series), in accordance with the corresponding crystallite dimensions. Indeed, since a PDF pattern reflects the density of the repetition of atomic configuration, the PDF signal weakens as  $r$  approaches the crystallite dimension, and eventually completely disappears when  $r$  exceeds the crystallite dimension. Note that the first and the second peaks are not affected by any types of disorder.

Each type of disorder affects specific atomic pairs. The impact is, however, not so distinctive as for PXRD. This is because one type of disorder affects several atom pairs simultaneously, and a single PDF peak is formed by the contribution of multiple atom pairs, (as shown by the simulated partial PDFs in top part of Figure 4. For example, the second PDF peak (at 0.35 nm) already contains the contribution of Cl-Cl and Mg-Mg pairs. Qualitative discussion on the impact of different types of disorder on a PDF pattern is not so straightforward as for PXRD, except for crystallite miniaturization. Thus, computer-aided fitting with a structure model is indispensable for the interpretation of PDFs.

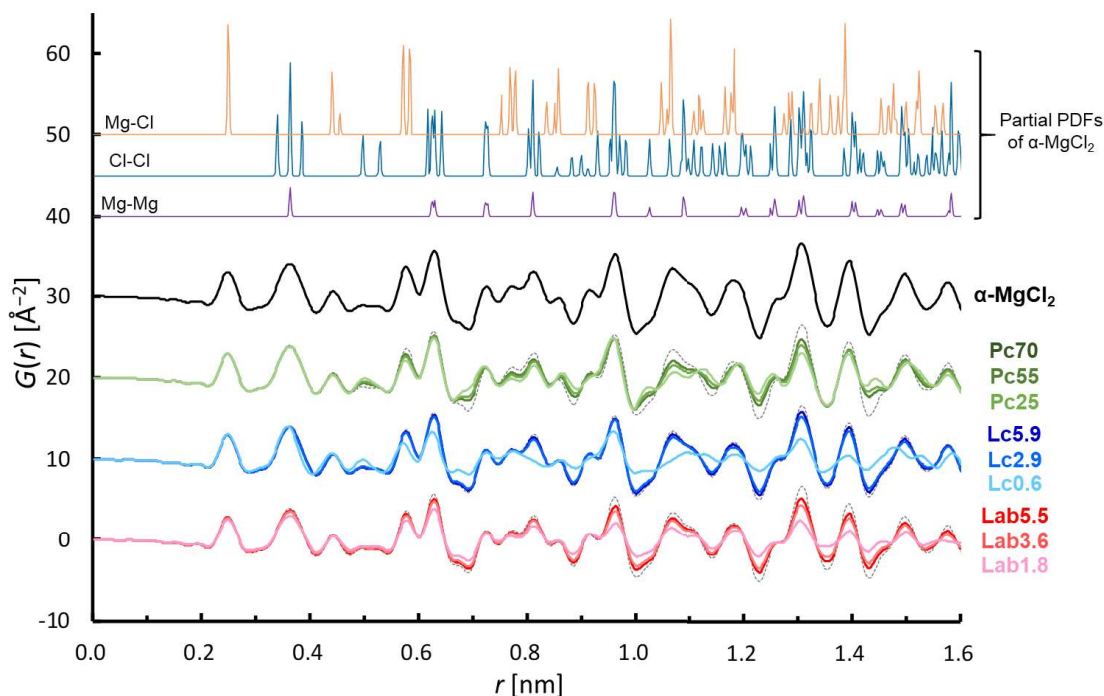


**Figure 4.** Simulated PDF patterns using  $\text{MgCl}_2$  nanoparticle models with various types and extents of disorder, as listed in Table 1. The simulation was performed using DISCUS ( $Q_{\text{max}} = 15 \text{ \AA}^{-1}$ ). For comparison, the simulated PDF of  $\alpha\text{-MgCl}_2$  is overlaid as a dotted line. Partial PDFs for each possible atomic pair in the  $\alpha\text{-MgCl}_2$  nanoparticle model are also given at the top of the graph. The simulated PDFs are vertically translated for clarity.

### 3.4 Analysis of the experimental PDF patterns

Figure 5 summarizes the PDF patterns of the four samples acquired from the synchrotron total scattering data. They are represented separately for long-range and short-range regions in Figure 5A and 5B, respectively. The long-range region is useful to evaluate the crystallite dimensions. For instance, MgCl<sub>2</sub> A shows almost no damping in this range, suggesting that its crystallite dimension is sufficiently larger than 10 nm and the occurrence of stacking error is negligible. On the other hand, the other three samples show an intensity decay along with  $r$ . Since MgCl<sub>2</sub> B and C do not completely lose intensity even when  $r$  reaches 10 nm, the crystallite dimension is considered to be over 10 nm. The PDF of ZNC completely diminishes at  $r = 5\text{--}8$  nm, indicating the crystallite dimensions are below 5-8 nm. These results well agree with the PXRD-determined crystallite dimensions of individual samples.

In the short-range region, the PDFs are damped in the order of MgCl<sub>2</sub> A, B, C, and ZNC. As discussed above, this damping of the PDFs should be caused by mix contribution of the three types of disorder. On the other hand, the position and broadness of the first nearest peak are found to be unchanged among the four samples (e.g. the position lies in  $0.250 \pm 0.001$  nm). This fact indicates that the stacking disorder as well as the crystallite miniaturization hardly introduces lattice distortion in MgCl<sub>2</sub>, even though the crystallite dimension of ZNC (lower than 10 nm) is analogous to the typical size of the occurrence of lattice distortion in the case of metal or metal oxide nanoparticles [51]. The ionic nature of the MgCl<sub>2</sub> crystal as well as the surface capping by TiCl<sub>4</sub> and donor molecules [52] likely accounts for this observation.

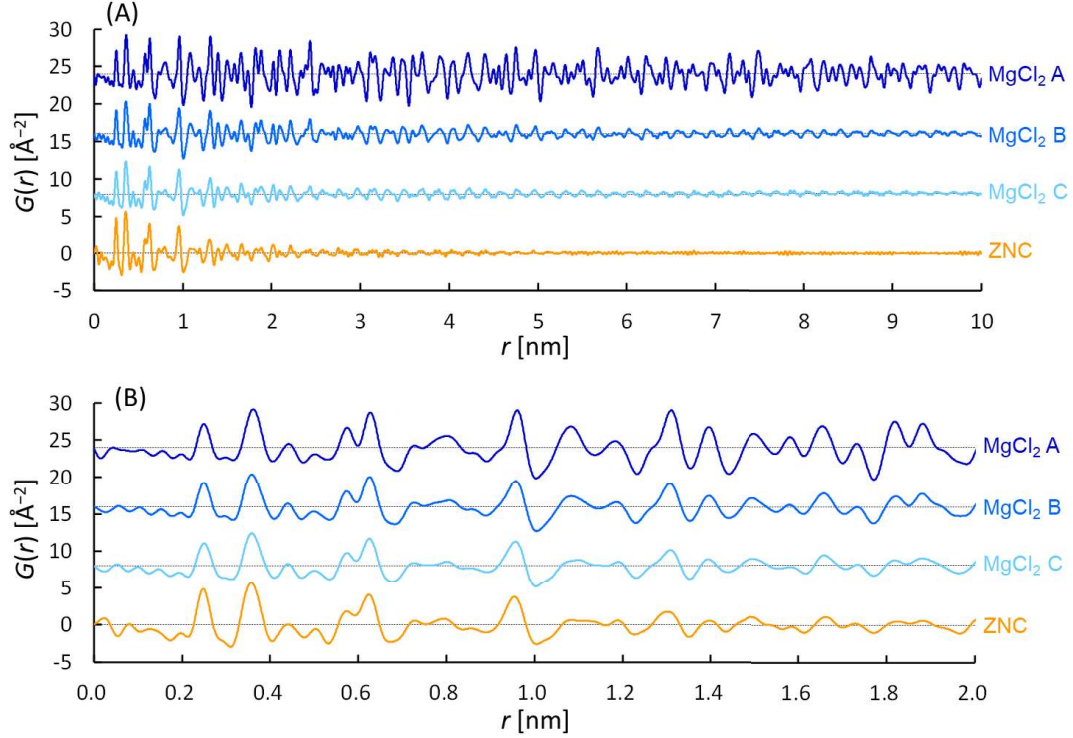


**Figure 5.** PDFs of mechanically and chemically activated  $\delta$ -MgCl<sub>2</sub>. The PDFs are shown in A) long-range and B) short-range regions.

As a final step, PDF fitting was performed using the same nanoparticle models discussed so far. The structural parameters were optimized in order to minimize the  $R_{w,PDF}$  value. Briefly, only the lattice constants ( $l_a, l_b, l_c$ ) were optimized for MgCl<sub>2</sub> A assuming an infinite  $\alpha$ -crystal of MgCl<sub>2</sub>.  $P_c, l_a, l_b, l_c$  and  $D$  (corresponding to the crystallite dimension within a spherical approximation) were optimized for the relatively isotropic MgCl<sub>2</sub> B and C samples.  $L_a, L_b, L_c$ , and  $P_c$  were explicitly optimized for ZNC. Note that internal parameters related to  $\sigma_{ij}$  of Equation (6) were internally optimized for each nanoparticle model. The fitting results are summarized in Figure 6 and Table S2. As can be seen, satisfactory agreements were obtained between the experimental and simulated PDFs with the  $R_{w,PDF}$  values below 0.3. In particular, the intensity damping observed in MgCl<sub>2</sub> B and C were adequately reproduced based on the

cutoff diameter ( $D$ ) of 18.7 and 13.7 nm, respectively. The corresponding particle volumes were highly consistent with those calculated from the PXRD-determined dimensional parameters (reported in Table 3). The damping feature of the experimental PDF of ZNC was also well reproduced with the simulation.

### 3.5 Cross-validation by combining PXRD and PDF

As stated in the experimental section, the PDF fitting has a larger number of fitting parameters compared to the PXRD fitting, and it could be doubted if these parameters would compromise the specificity of the determined nanoparticle model. However, it must be stressed that the best nanoparticle models proposed from PDF fitting well matched with the corresponding nanoparticle models in PXRD. For example, Figure S2 shows that deviation from the best-fit model monotonously deteriorated the fitting quality. Herewith, structure determination of  $\delta$ -MgCl<sub>2</sub> was first accomplished in a cross-validated manner.

As a final comment, the cross-validation by the combination of PXRD, PDF, and molecular simulation is a powerful method not only for structure determination of  $\delta$ -MgCl<sub>2</sub>, but also for verification of other disorder models. For instance, Di Noto et al. demonstrated that a MgCl<sub>2</sub> nanoribbon or a polymeric MgCl<sub>2</sub> structure also can reproduce a diffuse PXRD pattern, but this statement was not verified by another analytical method [26]. As a natural consequence of one-dimensional structure, such structures should have a decreasing atomic density over the second coordination sphere. Hence, we created three nanoparticle models for one-dimensional MgCl<sub>2</sub>, and simulated their PDFs (Figure 7). As expected, the relative intensity of the second nearest peak is obviously smaller than that observed in the experimental PDF of ZNC. The damping along with  $r$  is also much faster due to the decreasing atomic density. Thus, chain-like MgCl<sub>2</sub> structures can be excluded as models of ZNC. It is worth noticing that this conclusion is limited to the Mg(OEt)<sub>2</sub>-derived catalyst

systems. Such a structure may exist for other ZNCs, especially when the extent of the dealcoholation is sufficiently low for the  $\text{MgCl}_2$ -alcohol system. This is another interesting issue to be addressed in forthcoming studies.

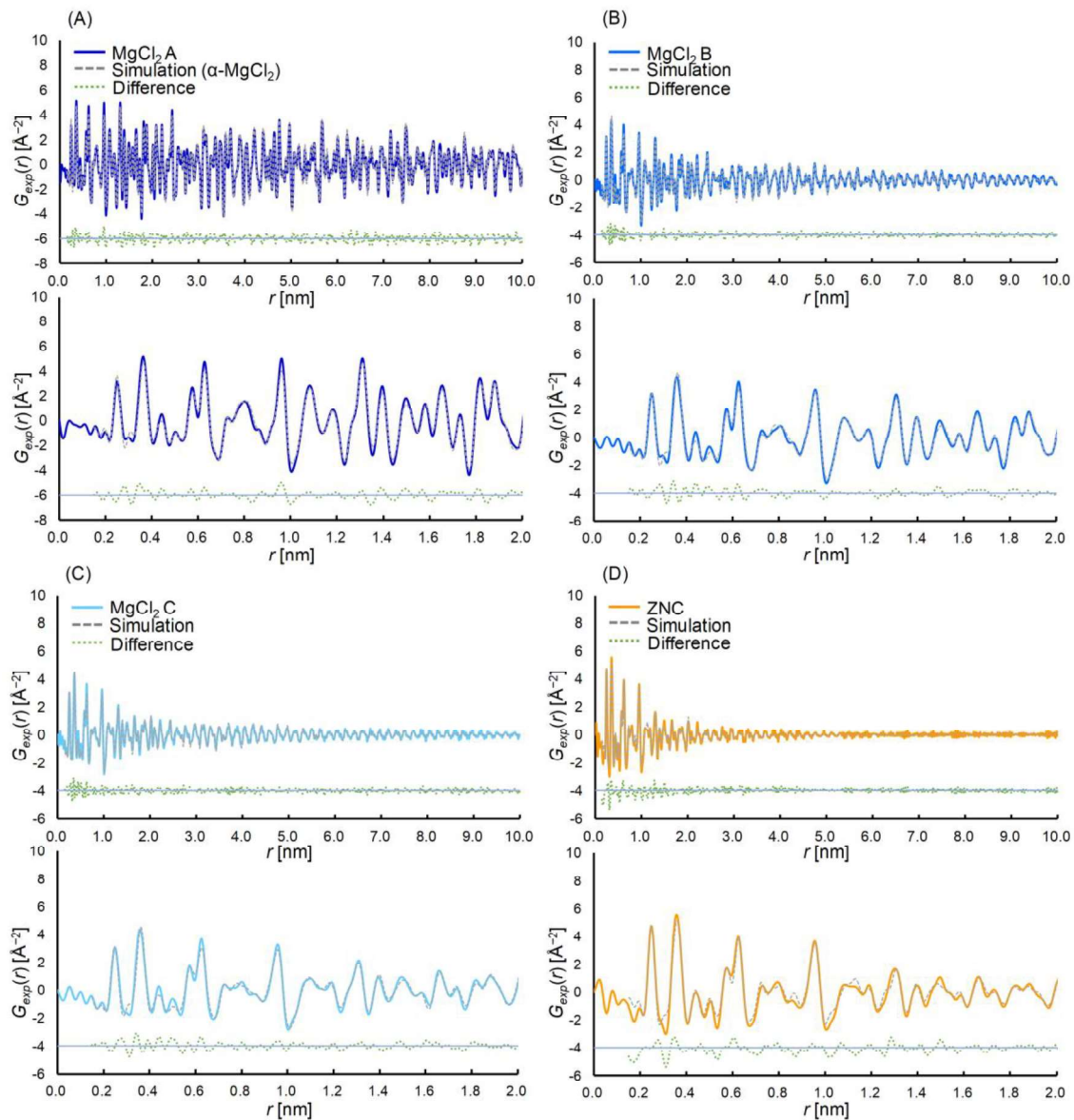


**Figure 6.** PDF fitting results. The difference between the experimental and simulated patterns is shown as a green dotted line.



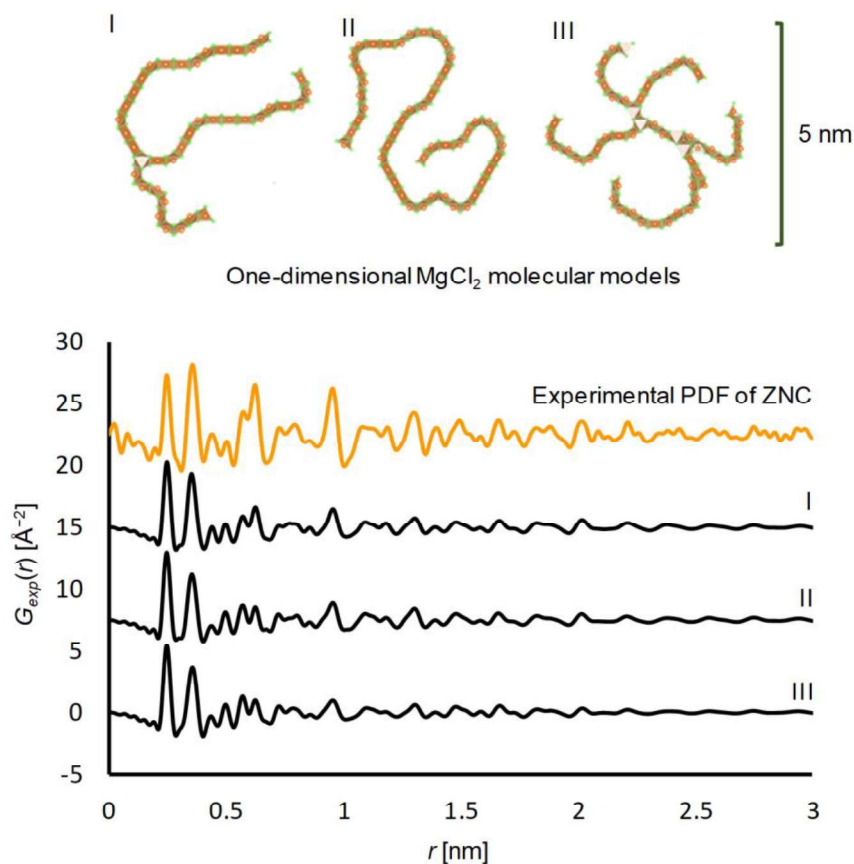


**Figure 7.** Simulated PDF of one-dimensional  $\text{MgCl}_2$  nanoparticle models I, II, and III. The experimental PDF of ZNC is also shown as a reference.

#### 4. CONCLUSIONS

A detailed structural analysis of disordered  $\delta\text{-MgCl}_2$  in heterogeneous Ziegler-Natta catalysts (ZNCs) was performed by synchrotron X-ray total scattering. Molecular simulation aided the understanding of the impact of different types of disorder on powder X-ray diffraction (PXRD) and pair distribution function (PDF), which is fundamental for a comprehensive interpretation of the experimental results. By combining PXRD, PDF, and molecular simulation, consistent nanoparticle models were derived respectively for mechanically and chemically activated  $\delta\text{-MgCl}_2$ . The results supported the conventional

hypothesis that  $\delta$ -MgCl<sub>2</sub> consists of disorderedly stacked nanoplates. Nevertheless, this study is the first attempt of applying synchrotron X-ray total scattering technique to clarify the structure of  $\delta$ -MgCl<sub>2</sub> in a cross-validated manner.

Although it is widely recognized that the activation of MgCl<sub>2</sub> is an essential step for improving the catalytic performances of ZNCs, the so formed  $\delta$ -MgCl<sub>2</sub> was never sufficiently characterized because of certain difficulties in the experimental investigation. The structural method presented in this study, based on the combination of PXRD, PDF, and simulation, together with the surface analysis tackled in the second part of this work [32], shed a new light for this long-standing problem, defining the dimension, disorder, and morphology of  $\delta$ -MgCl<sub>2</sub> in ZNCs.

#### AUTHOR INFORMATION

##### **Corresponding Author**

\*E-mail: [taniike@jaist.ac.jp](mailto:taniike@jaist.ac.jp)

##### **Author Contribution**

T.W. performed the experiments as well as the simulation works. G.T. created some nanoparticle models and helped computational simulation. A.P., M.D., A.T., P.C., P.C.B., M.T., B.C., S.B., and E.G. made analytical works and important suggestions in the framework of this collaboration. T.T. conceived the concept and supervised the entire research.

##### **Notes**

The authors declare no competing financial interest.

## Acknowledgements

The X-ray total scattering experiments were conducted at the BL5S2 of Aichi Synchrotron Radiation Center, Aichi Science & Technology Foundation, Aichi, Japan (proposal numbers: 201706107 and 201706157). The work of T.W., A.P., C.P., M.T., E.G., and T.T. forms part of the research programme of DPI, project #802.

## REFERENCES

- [1] P.L. Gai-Boyes, *Catal. Rev.* 34 (1992) 1–54.
- [2] A.T. Bell, *Science* (80-. ). 299 (2003) 1688–1691.
- [3] M. Behrens, F. Studt, I. Kasatkin, S. Kuhl, M. Havecker, F. Abild-Pedersen, S. Zander, F. Girgsdies, P. Kurr, B.-L. Kniep, M. Tovar, R.W. Fischer, J.K. Norskov, R. Schlogl, *Science* (80-. ). 336 (2012) 893–897.
- [4] B. Roldan Cuenya, F. Behafarid, *Surf. Sci. Rep.* 70 (2015) 135–187.
- [5] S.J.L. Billinge, *J. Solid State Chem.* 181 (2008) 1695–1700.
- [6] L. Noristi, E. Marchetti, G. Baruzzi, P. Sgarzi, *J. Polym. Sci. Part A Polym. Chem.* 32 (1994) 3047–3059.
- [7] V. Busico, M. Causà, R. Cipullo, R. Credendino, F. Cutillo, N. Friederichs, R. Lamanna, A. Segre, V. Van Axel Castelli, *J. Phys. Chem. C.* 112 (2008) 1081–1089.

- [8] T. Taniike, V.Q. Thang, N.T. Binh, Y. Hiraoka, T. Uozumi, M. Terano, *Macromol. Chem. Phys.* 212 (2011) 723–729.
- [9] T. Taniike, T. Funako, M. Terano, *J. Catal.* 311 (2014) 33–40.
- [10] E.S. (Merijn) Blaakmeer, G. Antinucci, V. Busico, E.R.H. van Eck, A.P.M. Kentgens, *J. Phys. Chem. C.* 120 (2016) 6063–6074.
- [11] P. Chammingkwan, M. Terano, T. Taniike, *ACS Comb. Sci.* 19 (2017) 331–342.
- [12] E. Breuza, G. Antinucci, P.H.M. Budzelaar, V. Busico, A. Correa, C. Ehm, *J. Phys. Chem. C.* 122 (2018) 9046–9053.
- [13] T. Taniike, M. Terano, The Use of Donors to Increase the Isotacticity of Polypropylene, in: *Adv. Comput. Simul. Approaches Soft Matter Sci. I*, 2013: pp. 81–97.
- [14] B. Keszler, G. Bodor, A. Simon, *Polym. (United Kingdom)*. 21 (1980) 1037–1040.
- [15] J.C.J. Bart, *J. Mater. Sci.* 28 (1993) 278–284.
- [16] V. Di Noto, S. Bresadola, *Macromol. Chem. Phys.* 197 (1996) 3827–3835.
- [17] M. Chang, X. Liu, P.J. Nelson, G.R. Munzing, T.A. Gegan, Y. V. Kissin, *J. Catal.* 239 (2006) 347–353.
- [18] A. Martorana, R. Zannetti, A. Marigo, D. Ajò, V. Malta, *Comput. Phys. Commun.* 27 (1982) 49–55.
- [19] P. Gall, P. Barbi, R. Zannetti, A. Martorana, A. Marigo, A. Fichera, V. Loredan, *Eur. Polym. J.* 19 (1983) 19–24.
- [20] G. Giunchi, G. Allegra, *J. Appl. Crystallogr.* 17 (1983) 172–178.

- [21] R. Zannetti, C. Marega, A. Marigo, A. Martorana, *J. Polym. Sci. Part B Polym. Phys.* 26 (1988) 2399–2412.
- [22] A. Marigo, C. Marega, R. Zannetti, G. Morini, G. Ferrara, *Eur. Polym. J.* 36 (2000) 1921–1926.
- [23] D. Fregonese, S. Bresadola, *J. Mol. Catal. A Chem.* 145 (1999) 265–271.
- [24] E. Redzic, T. Garoff, C.C. Mardare, M. List, G. Hesser, L. Mayrhofer, A.W. Hassel, C. Paulik, *Iran. Polym. J. (English Ed.)* 25 (2016) 321–337.
- [25] G.D. Bukatov, D.K. Maslov, S.A. Sergeev, M.A. Matsko, *Appl. Catal. A Gen.* 577 (2019) 69–75.
- [26] S. Suarez, V. Di Noto, P.E. Stallworth, S. Abbrent, M. Vittadello, F.M. Alamgir, S.G. Greenbaum, C.M. Drain, *Inorganica Chim. Acta.* 359 (2006) 2513–2518.
- [27] P. Thompson, D.E. Cox, J.B. Hastings, *J. Appl. Crystallogr.* 20 (1987) 79–83.
- [28] R.W. Berg, F.W. Poulsen, K. Nielsen, *Acta Chem. Scand.* 51 (1997) 442–448.
- [29] R. Guinebretière, A. Boulle, O. Masson, A. Dauger, *Powder Diffr.* 20 (2005) 294–305.
- [30] T. Egami, S.J.L. Billinge, *Underneath the Bragg peaks: structural analysis of complex materials*, Newnes, 2012.
- [31] *J. Appl. Crystallogr.* 12 (1979) 34–38.
- [32] A. Piovano, M. D'Amore, T. Wada, P.C. Bruzzese, G. Takasao, A. Thakur, P. Chammingkwan, M. Terano, B. Civalieri, S. Bordiga, T. Taniike, E. Groppo, *J. Catal.* submitted (2020).
- [33] M. Terano, H. Soga, *CATALYST FOR POLYMERIZATION OF OLEFINS US*, 1989.

- [34] A. Dashti, A. Ramazani SA, Y. Hiraoka, S.Y. Kim, T. Taniike, M. Terano, *Polym. Int.* 58 (2009) 40–45.
- [35] Y. Hiraoka, S.Y. Kim, A. Dashti, T. Taniike, M. Terano, *Macromol. React. Eng.* 4 (2010) 510–515.
- [36] T. Funako, P. Chammingkwan, T. Taniike, M. Terano, *Macromol. React. Eng.* 9 (2015) 325–332.
- [37] T. Proffen, R.B. Neder, *J. Appl. Crystallogr.* 32 (1999) 838–839.
- [38] D.E. Partin, M. O’Keeffe, *J. Solid State Chem.* 95 (1991) 176–183.
- [39] T. Taniike, M. Terano, *J. Catal.* 293 (2012) 39–50.
- [40] G. Takasao, T. Wada, A. Thakur, P. Chammingkwan, M. Terano, T. Taniike, *ACS Catal.* (2019).
- [41] K. Momma, F. Izumi, *J. Appl. Crystallogr.* 44 (2011) 1272–1276.
- [42] P. Scardi, S.J.L. Billinge, R. Neder, A. Cervellino, *Acta Crystallogr. Sect. A Found. Adv.* 72 (2016) 589–590.
- [43] X. Qiu, J.W. Thompson, S.J.L. Billinge, *J. Appl. Crystallogr.* 37 (2004) 678–678.
- [44] E.S. Božin, S.J.L. Billinge, T. Proffen, C.L. Farrow, P. Juhas, D. Bryndin, J.W. Liu, J. Bloch, *J. Phys. Condens. Matter.* 19 (2007) 335219.
- [45] D. Olds, H.-W. Wang, K. Page, *J. Appl. Crystallogr.* 48 (2015) 1651–1659.
- [46] A.S. Masadeh, E.S. Božin, C.L. Farrow, G. Paglia, P. Juhas, S.J.L. Billinge, A. Karkamkar, M.G. Kanatzidis, *Phys. Rev. B - Condens. Matter Mater. Phys.* 76 (2007) 1–11.

- [47] C.L. Farrow, D.K. Bediako, Y. Surendranath, D.G. Nocera, S.J.L. Billinge, *J. Am. Chem. Soc.* 135 (2013) 6403–6406.
- [48] M.W. Terban, C. Shi, R. Silbernagel, A. Clearfield, S.J.L. Billinge, *Inorg. Chem.* 56 (2017) 8837–8846.
- [49] B.E. Warren, *Phys. Rev.* 59 (1941) 693–698.
- [50] P. Chammingkwan, V.Q. Thang, M. Terano, T. Taniike, *Top. Catal.* 57 (2014) 911–917.
- [51] V. Swamy, D. Menzies, B.C. Muddle, A. Kuznetsov, L.S. Dubrovinsky, Q. Dai, V. Dmitriev, *Appl. Phys. Lett.* 88 (2006) 2004–2007.
- [52] R. Credendino, J.T.M. Pater, A. Correa, G. Morini, L. Cavallo, *J. Phys. Chem. C* 115 (2011) 13322–13328.

# Supplementary material

## Revisiting the identity of $\delta$ -MgCl<sub>2</sub>: Part I. Structural disorder studied by synchrotron X-ray total scattering

*Toru Wada<sup>†,§</sup>, Gentoku Takasao<sup>†</sup>, Alessandro Piovano<sup>‡,§</sup>, Maddalena D'Amore<sup>‡</sup>,  
Ashutosh Thakur<sup>†</sup>, Patchanee Chammingkwan<sup>†,§</sup>, Paolo Cleto Bruzzese<sup>‡</sup>, Minoru Terano<sup>†,§</sup>,  
Bartolomeo Civalleri<sup>‡</sup>, Silvia Bordiga<sup>‡,§</sup>, Elena Groppo<sup>‡,§</sup> and Toshiaki Taniike<sup>\*,†,§</sup>*

<sup>†</sup>Graduate School of Advanced Science and Technology, Japan Advanced Institute of Science  
and Technology, 1-1 Asahidai, Nomi, Ishikawa, 923-1292, Japan

<sup>‡</sup>Department of Chemistry, INSTM and NIS Centre, University of Torino, Via Giuria 7,  
10125 Torino, Italy

<sup>§</sup>Dutch Polymer Institute, P.O. Box 902, 5600 AX Eindhoven, the Netherlands

\*Corresponding author. E-mail: taniike@jaist.ac.jp



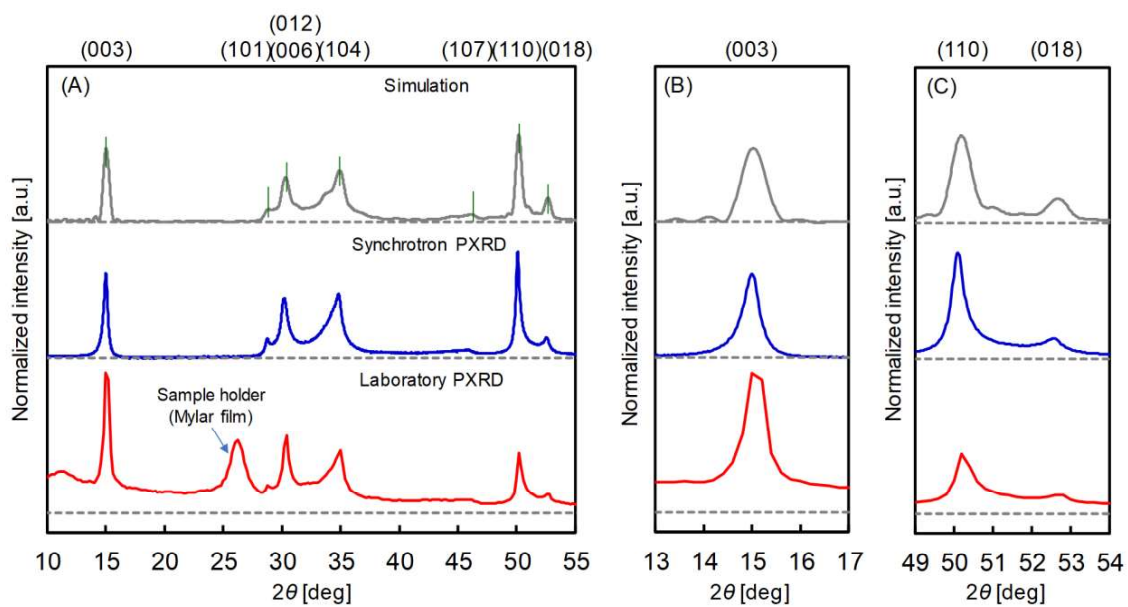


**Figure S1.** Comparison of laboratory and synchrotron PXRD with a simulated diffraction pattern. The measured sample was  $\text{MgCl}_2 \text{ B}$ . Results in A) the whole and B,C) narrow ranges of  $2\theta$ .

**Table S1.** Results of PDF fitting with PDFgui.

Parameter	MgCl <sub>2</sub> A	MgCl <sub>2</sub> B	MgCl <sub>2</sub> C	ZNC
$R_{w,PDF}$	0.1751	0.2126	0.2521	0.2716
ADP:				
$U_{11,Mg}, U_{22,Mg}$ [nm <sup>2</sup> ]	0.000092	0.000176	0.000183	0.000120
$U_{33,Mg}$ [nm <sup>2</sup> ]	0.000785	0.000826	0.000143	0.000758
$U_{11,Cl}, U_{22,Cl}$ [nm <sup>2</sup> ]	0.000093	0.000195	0.000176	0.000133
$U_{33,Cl}$ [nm <sup>2</sup> ]	0.000488	0.000615	0.001246	0.000156
Scale factor				
	0.9458	1.1285	1.2447	1.4660
$Q_{damp}$ [nm <sup>-1</sup> ] <sup>a</sup>	0.1160	0.1160	0.1160	0.1160
$\Delta l$ [nm]	0.2209	0.1971	0.1895	0.1940
Lattice parameter:				
$l_a = l_b$ [nm]	0.3642	0.3640	0.3639	0.3636
$l_c$ [nm]	5.9099 <sup>b</sup>	5.9158 <sup>b</sup>	5.9145 <sup>b</sup>	0.5889
$D$ [nm] <sup>c</sup>	n.a.	18.7191	13.6582	n.a.

<sup>a</sup>  $Q_{damp}$  is an instrument-dependent parameter. It was determined using a standard sample and fixed as constant in the fitting.

<sup>b</sup>  $l_c$  was defined by the separation of neighboring Cl-Mg-Cl layers. See the main text for details.

<sup>c</sup>  $D$  is a fittable parameter to express the diameter of the model. This is a built-in function of PDFgui and widely applied for isotropic nanomaterials.

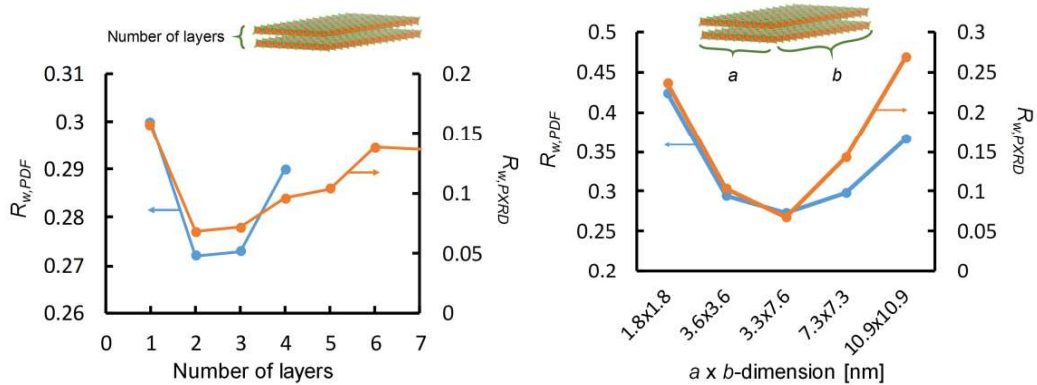
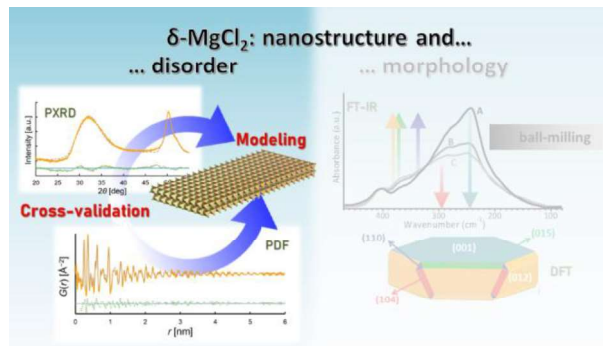


**Figure S2.**  $R_{w,PDF}$  and  $R_{w,PXRd}$  values when structural parameters are varied for ZNC. Note that PXRd and PDF fitting gave a consistent nanoparticle model.

# Graphical abstract



## Research highlights

- Quantitative structural determination of  $\delta$ -MgCl<sub>2</sub> for Ziegler-Natta catalysts.
- The first example of synchrotron X-ray total scattering on  $\delta$ -MgCl<sub>2</sub>.
- Combinatorial usage of PXRD, pair distribution function, and molecular simulation.